Ecotoxicology and Environmental Safety 304 (2025) 119075

Contents lists available at ScienceDirect

Ecotoxicology and Environmental Safety

journal homepage: www.elsevier.com/locate/ecoenv

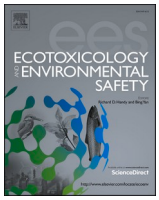

The role of methodological conditions and model interpretation in the adsorption of a nanomaterial on a volcanic soil

Manuel Gacitua [a,b], Angelo Neira-Albornoz [c,*]

[a] Facultad de Ingeniería y Ciencias, Universidad Diego Portales,, Av. Ejército Libertador 441, Santiago 8370191, Chile
[b] Centro Para El Desarrollo de La Nanociencia Y Nanotecnología (CEDENNA), Av. L.B. O'Higgins 3363, Santiago 7254758, Chile
[c] Zukunftskolleg, University of Konstanz, Universitaetsstrasse 10, Konstanz 78464, Germany

ARTICLE INFO

Edited by Tao Zhang

Keywords:
Nanomaterial
Volcanic soil
Pseudo-second order
Langmuir
Freundlich
Data production
Model interpretation

ABSTRACT

Soil adsorption governs the environmental fate of nanomaterials, yet standard procedures often fail to fully capture adsorption behaviour through kinetic and isotherm models. This study proposes a comprehensive framework to enhance the reliability and interpretability of adsorption data by improving both experimental design and model analysis, using the adsorption of Cu_2O nanoparticles from the commercial pesticide NORDOX 75 WG (NOR) in Metrenco soil (Ultisol). Batch adsorption kinetics and isotherm experiments were conducted. NOR stability and supernatant pH were the most influential factors and were used to select a subset of consistent, comparable data. Transport-related parameters (e.g., kinetic rates) were more sensitive to NOR stability than bulk-adsorbent parameters (e.g., adsorption capacity). We applied a novel validation strategy combining traditional goodness-of-fit metrics (including adjusted R^2) with intra-model assumption checking, and inter-model comparison. While the linear Pseudo-Second Order model (PSO) achieved the highest R^2_{adj}, a combined analysis of multiple nonlinear models provided stronger evidence for non-equilibrium condition and apparent instantaneous adsorption, in contrast to the interpretation derived from linear PSO parameters. This approach also led to the formulation of a modified PSO model equation, better aligned with the system behaviour and consistent with trends observed in other models. Unlike typical studies that rely on a single "best-fitting" model, our method enables deeper mechanistic insights, even from poorly fitting models. This addresses a widespread but overlooked issue in the literature and supports more robust modelling of complex adsorption systems to support environmental decision-making.

1. Introduction

Understanding soil adsorption is a key process for predicting the environmental fate of pollutants (Neira-Albornoz et al., 2022). This process is commonly studied through the batch equilibrium method, as proposed by the Organisation for Economic Co-operation and Development (OECD, 2000). Because the representational value of adsorption data depends on methodological and contextual factors, its applicability to real-world environmental scenarios must be critically assessed and validated in each study to inform decision-makers effectively (Neira-Albornoz et al., 2022, 2024).

Two main stages are especially relevant for evaluating the applicability of adsorption data: (i) data production and (ii) data interpretation. In batch studies, data production relies on methodological conditions such as soil/solution ratio, appropriate contact time to ensure equilibrium, analyte stability to ensure a correct mass balance, and reliable analytical methods (OECD, 2000). Equally important, data interpretation involves applying kinetic and isotherm models with distinct assumptions, but model selection is often based solely on the coefficient of determination (R^2), despite its limitations as a validation tool (Revellame et al., 2020).

This narrow focus on R^2 as the primary model selection criterion is widespread in the literature. Many studies rely exclusively on R^2 Khepar et al., (2024); Lu et al., (2021); Rahman et al., (2019); Lim and Lee (2015), while others incorporate additional statistical metrics but still identify a single "best" model based on the highest goodness-of-fit (Salvestrini et al., 2014). In most cases, only the best-fitting models are interpreted, often in isolation (Rahman et al., 2019; Lim and Lee, 2015; Quesada-Peñate et al., 2009; Sharma and Chaudhary, 2025), potentially missing mechanistic insights provided by models with lower

* Corresponding author.
E-mail addresses: manuel.gacitua@mail.udp.cl (M. Gacitua), angelo.neira@uni-konstanz.de (A. Neira-Albornoz).

https://doi.org/10.1016/j.ecoenv.2025.119075
Received 14 February 2025; Received in revised form 21 May 2025; Accepted 15 September 2025
Available online 17 September 2025

fit quality or by comparing multiple models in combination. Notably, this issue spans across publication years and impact levels, including highly cited and recent studies for different sorbents and pollutants. This suggests a systemic pattern in the literature, not a problem confined to outdated or low-quality research.

In this context, the present study introduces a more comprehensive model evaluation framework that integrates traditional goodness-of-fit metrics with intra-model validation (consistency with model assumptions) and inter-model validation (cross-model comparison of shared assumptions). This approach allows for a more robust interpretation of adsorption mechanisms and enables valuable insights even from models with low statistical performance, which are typically disregarded. By doing so, the study challenges the conventional "best model" approach and emphasizes interpretive depth over statistical ranking.

The need for improved methodological rigor is especially pressing in the case of nanomaterials. They are globally employed (Fortune-Business-Insights, 2024), their release into the environment has raised significant concerns as emerging soil pollutants (Kiaune and Singhasemanon, 2011), and their adsorption behaviour is highly sensitive to soil physicochemical properties such as organic carbon (OC) content, pH and amorphous Fe (Julich and Gäth, 2014; Sekine et al., 2017; Tegenaw et al., 2019). In particular, Cu oxide nanoparticles used in pesticides like NORDOX 75 WG (NOR), a commercial granulated water-dispersible pesticide containing Cu_2O as its active ingredient (Tomasgaard et al., 2004), have been shown to affect environmental fate, plant growth, mobility and bioavailability depending on their particle size and composition (Kiaune and Singhasemanon, 2011; Burachevskaya et al., 2021; Manzoor et al., 2023).

Therefore, this study aims to evaluate how current experimental and modelling practices influence the representativeness and applicability of adsorption data in complex systems. We examined (i) the impact of methodological decisions on data production and interpretation, and (ii) the conceptual alignment between model assumptions and methodological conditions to apply these models. This includes assessing the validity of quantification methods, the suitability of experimental conditions, and the use of models not just as curve-fitting tools, but as conceptual representations of adsorption processes.

2. Materials and methods

2.1. Soils

A volcanic soil from the southern central area of Chile an unfertilized Metrenco soil sample (38°34' S; 72°22' W) was chosen. The sample was collected at a depth of 0–15 cm and stored at field moisture. This soil belongs to the Ultisol series, vastly reported on past studies (Table 1), and has been thoroughly characterized on many adsorption studies reported before (Cáceres-Jensen et al., 2013; Cáceres et al., 2010a, 2010b; Báez et al., 2015; Caceres-Jensen et al., 2019).

Metrenco is characterized as a silty clay loam soil, with low OC content and acid pH. EC was measured at the supernatant in the same soil:solution mixture with distilled water after a 10 min centrifugation (8000 rpm) step (Sadzawka, 1991). IEP was measured through the electrophoretic mobility of samples suspended in 10^{-3} M NaCl in a Zeta meter where pH was adjusted with 10^{-2} M HCl or NaOH (Hunter, 1981).

According to inorganic contents on Metrenco soil there are less than 0.2 wt% of non-characterized oxides. Thus, the possibility of finding Cu_2O particles native to the soil are negligible.

2.2. NORDOX suspension

According to the manufacturer, NOR contains approximately 84 % Cu_2O nanoparticles as its main active ingredient. Other components include unspecific wetting agents, dispersants, disintegrants, binders and buffering agents (Tomasgaard et al., 2004). While these additives may influence the adsorption processes, these effects cannot be determined without knowledge of their composition or proportion.

NOR suspension was made by mixing a certain amount of the product in distilled water. After vigorous mixing, the mix is centrifuged at 10,000 rpm for 30 min. The supernatant is recovered, and vacuum filtrated using a nitrocellulose 1.0 micrometer filter. The filtered suspension is then diluted to a desired concentration by means of a UV visible spectrophotometer. Absorbance values provided by spectrophotometer were denoted by the letter S and interpreted as the sum between scattered and the adsorbed light by the NOR particle suspension. Solutions were prepared to fixed S values (ranging from 0 to 0.900) at 490 nm wavelength. NOR suspensions in deionized water were prepared daily to ensure its stability and repeatability of results. Aliquots of adequate volumes for each solution were transferred in triplicate to tared beakers and placed in lab-oven at 85 °C until reaching constant mass. Beakers were weighted to obtain the mass from dry NOR particles, and a calibration curve was constructed to check the dependence between S and mass concentration (mg L^{-1}) of NOR suspension. Calibration curve construction for nanoparticle suspensions has been reported before for different systems (Gacitua et al., 2022; Escudey et al., 2025).

2.3. Adsorption experiments

2.3.1. Experimental points construction

The method for adsorption points construction from particle suspension has been reported before (Gacitua et al., 2022). Summarizing, groups of five 15 mL centrifuge tubes were prepared at the same time to quantify S following three independent combinations (Fig. 1). First, three centrifuge flasks contained a volume V = 12 mL of NOR suspension or distilled water into a mass m_{soil} = 1.2 g of air-dry soil (solution: soil ratio = 10:1), used to evaluate the adsorption of NOR on Metrenco soil (S_{NOR}, triplicate). Another flask contained the NOR suspension alone to check its stability through the duration of the experiment by quantifying the amount of NOR at the beginning and the end of the study (as $S_{0(start)}$ and $S_{0(end)}$, respectively). Finally, the last flask contained 1.2 g of soil and 12 mL of water (without NOR) to check for the liberation of unspecific soil particles (S_{soil}, soil interference) during the experiment.

The set of flasks were agitated in an orbital shaker at 65 rpm at room temperature. Then the flasks were centrifuged at 10,000 rpm for 10 min. The liquid supernatant was filtered using 1.0 μm syringe filters and the filtered liquid was controlled by UV–visible light spectrophotometer at 490 nm.

According to the Lambert-Beer law, absorbance S is linked to the concentration of NOR (C_0 from S_0), NOR + interference (C_{NOR} from S_{NOR}), and interference (C_{soil} from S_{soil}). In this sense, the adsorbed

Table 1
Metrenco soil properties (Sadzawka, 1991; Besoain, 1985; Hunter, 1981).

Texture (wt%)			OC[a] (wt%)	pH-H_2O	EC[a] (dS m^{-a})	IEP[a]	Porosity (%)	Dominant Mineralogy	> 50 % Halloysite
Sand	Silt	Clay							< 1 % Goethite
8	56.7	35.3	2.3	4.7	0.04	2.2	45		< 1 % Quartz
Inorganic contents (wt%)									
SiO_2	TiO_2	Al_2O_3	Fe_2O_3	MnO_2	MgO	CaO	Na_2O	K_2O	P_2O_5
46.2	3.0	27.4	16.2	0.5	0.7	4.3	0.6	0.3	0.6

[a] **EC:** Electrical conductivity. **IEP:** Isoelectric point. **OC:** Organic carbon.

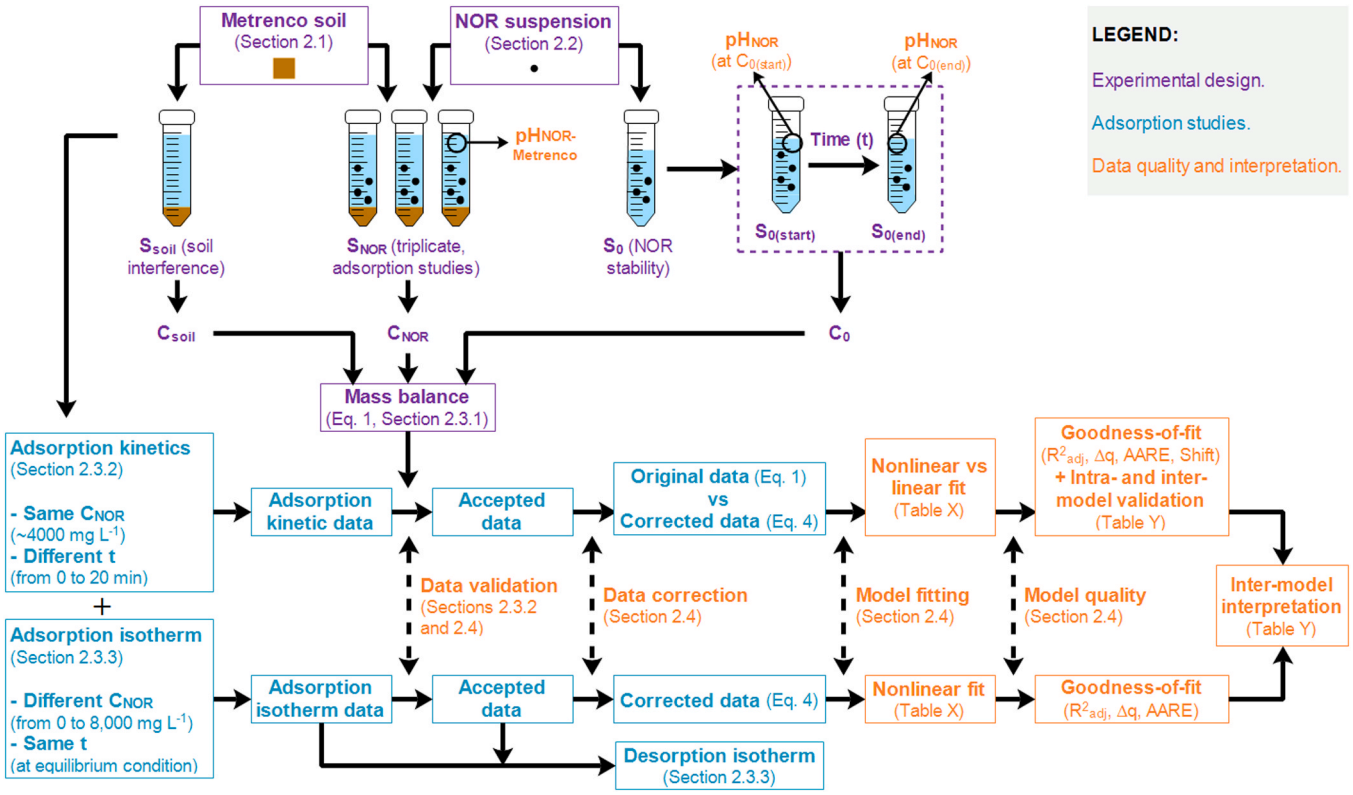

Fig. 1. Overview of the methodological workflow, divided into three topics: experimental design, adsorption studies, and data quality and interpretation (see legend). The sequence of methodological steps is indicated by arrows. References to relevant sections, equations and tables are provided throughout.

concentration of NOR on soils, $q_{ads(exp)}$, was indirectly quantified through a mass balance, if the difference between the initial (C_0) and final (C_{aq}) aqueous concentration of NOR was due to adsorption ($C_{ads(exp)}$) (Julich and Gäth, 2014).

$$q_{ads(exp)} = \left(\frac{V}{m_{soil}}\right) C_{ads(exp)} = \left(\frac{V}{m_{soil}}\right)(C_0 - C_{aq}) = \left(\frac{V}{m_{soil}}\right)(C_0 - (C_{NOR} - C_{soil})) \quad (1)$$

Where the value of C_{NOR} was calculated as the average between the replicates, and C_0 represents the average value between $C_{0(start)}$ and $C_{0(end)}$.

2.3.2. Adsorption kinetics

Adsorption kinetics studies were conducted over 7 days using a fixed initial NOR concentration ($C_0 \sim 4000$ mg L^{-1}), with experimental points evaluated at different contact times (0–20 min) until reaching stable NOR concentration left in solution (C_{aq}) (Fig. 1). However, to ensure comparability among kinetic data points collected at different times, C_0 must remain consistent across independent measurements. To address this, we applied correction factors to account for (i) the instability of NOR during the experiments (f_{sta}), and (ii) variations in C_0 across daily suspensions (f_{var}):

$$f_{sta} = \left(\frac{C_{0(start)}}{C_{0(end)}}\right) \quad (2)$$

$$f_{var} = \left(\frac{\overline{C}_0}{C_{0(start)}}\right), \text{where} \overline{C}_0 = \sum_{i=1}^{\#data}\left(\frac{C_{0(start\ i)}}{\#data}\right) \quad (3)$$

Where f_{sta} represents the deviation of $C_{0(end)}$ with respect to $C_{0(start)}$ due to instability, and f_{var} represents the deviation of $C_{0(start)}$ from the average and comparable value of $C_{0(start)}$ considering all experimental data.

Experimentally, data comparability depended on changes in (i) the adsorption process due to the difference between $C_{0(end)}$ and $C_{0(start)}$, and (ii) the adsorption trend (e.g., degree of nonlinearity) due to differences between $C_{0(start)}$ and $\overline{C}_0$. To minimise potential biases, we assumed that the smaller the difference between $C_{0(end)}$ and $C_{0(start)}$, and between $C_{0(start)}$ and $\overline{C}_0$, the more likely it is that data are described by the same adsorption trend.

In practical terms, we checked two conditions: (i) $0.95 \leq f_{sta} \leq 1.05$ and (ii) $|C_{0(start)} - \overline{C}_0| \leq SD(\overline{C}_0)$. We discarded data if the first condition was not met. Then, we checked the second condition and evaluated compensatory effects if $C_{0(start)} > C_{0(end)}$ ($f_{sta} > 1$) and $C_{0(start)} > \overline{C}_0$ ($f_{var} < 1$), discarding data only if there was no compensation, i.e., $0.95 \leq f_{sta} * f_{var} \leq 1.05$.

We used an average value of C_0 to quantify $q_{ads(exp)}$ (Eq. 1), assuming that this parameter better represents the concentration of NOR during the whole experiment. Therefore, we modified f_{sta} to f^*_{sta} by replacing $C_{0(end)}$ for C_0 in Eq. (2) and recalculated the accepted data as follows:

$$q_{ads(corr)} = q_{ads(exp)} * f^*_{sta} * f_{var} \quad (4)$$

From now on, $q_{ads(exp)}$ and $q_{ads(corr)}$ are associated to the original and recalculated data, respectively.

2.3.3. Adsorption-desorption isotherms

Adsorption isotherm studies were conducted over 15 days. Isothermal curve construction typically requires long durations, as varying concentrations introduce greater deviations due to pH changes and particle aggregation (Julich and Gäth, 2014). Although the manufacturer recommends preparing NOR suspensions up to 2500 mg L^{-1} (i.e., 250 g per 100 L), adsorption isotherm experiments were carried out using initial NOR concentrations ranging from 0 to 8000 mg L^{-1} to

ensure saturation and accurately estimate the maximum adsorbed concentration ($q_{ads(exp)}$). Optimal contact times, previously determined from kinetic studies as the closest to equilibrium while minimizing the impact of NOR instability (f_{sta}), were applied (Fig. 1).

Once the adsorption process had ended, and supernatants were removed, 12 mL of distilled water was added to remnant adsorbent to start the desorption experiment at $C_0 = 0$. The mixtures were subsequently agitated in an orbital shaker for 10 min at 65 rpm at room temperature. Finally, the flasks were centrifuged at 10,000 rpm for 10 min. The supernatants were filtered through a 1.0 μm pore-size syringe filter and the quantification of NOR was carried out in a UV/vis spectrophotometer at 490 nm.

Considering that f_{sta} presented a high variability among the experimental data, we only fitted models to corrected $q_{ads(corr)}$ data (Eq. 4). However, adsorption-desorption isotherms did not require corrected C_0 values, therefore, we assumed $f_{var} = 1$. The desorption percentage was quantified through the equation:

$$Des(\%) = 100 * \left(\frac{q_{ads(exp)} - q_{des(exp)}}{q_{ads(exp)}}\right) \quad (5)$$

$$q_{des(exp)} = \left(\frac{V}{m_{soil}}\right) C_{des(exp)} = \left(\frac{V}{m_{soil}}\right)(C_{NOR} - C_{soil}) \quad (6)$$

Where $q_{ads(exp)}$ and $q_{des(exp)}$ represent the values obtained from the adsorption and desorption experiment in the same centrifuge tube, respectively, assuming that differences between adsorption and desorption are due solely to desorption of NOR from soils. Eq. (6), was derived from Eq. (1) at $C_0 = 0$ and multiplying by -1 because desorption is the inverse to adsorption, i.e., the release of NOR from soils.

2.4. Data analysis

Prior to modeling, experimental data were validated assessing the effects of inter-day variability, contact time, C_0, pH and C_{soil} on NOR stability. Subsequently, the accepted adsorption (i) kinetic data in both original (Eq. 1) and corrected (Eq. 4) forms, and (ii) isotherm data in corrected form were fitted using various adsorption models (Table 2).

Following trends reported in the literature and considering the varying number of parameters across models, the adjusted correlation coefficient (R^2_{adj}) was selected as the primary indicator for goodness-of-fit (Khepar et al., 2024; Lu et al., 2021; Rahman et al., 2019; Lim and Lee, 2015). To complement it, we use with the normalised standard deviation (Δq) (Salvestrini et al., 2014):

$$\Delta q = \left(\frac{100}{n-1}\right) \sum_{i=1}^{n} \left(\frac{\left(y_{exp(i)} - y_{pred(i)}\right)^2}{y_{exp(i)}}\right) \quad (29)$$

Where n is the number of data points, and y_{exp} and y_{pred} are the experimental and predicted values for the response variable, respectively. In most cases, y_{exp} was q_t or q_{eq} (Table 2). However, for the TSNE model, the response variable was C_t and for linear models, it varied depending on the equation used. Consequently, Δq was not applied to these models. Instead, we used the average absolute relative errors (AARE) (Quesada-Peñate et al., 2009), a unit-invariant error metric:

$$AARE(\%) = \left(\frac{100}{n}\right) \sum_{i=1}^{n} \left(\frac{\left|y_{exp(i)} - y_{pred(i)}\right|}{y_{exp(i)}}\right) \quad (30)$$

Goodness-of-fit metrics (R^2_{adj}, Δq and AARE) were interpreted as indicators of information loss, where better fits correspond to higher R^2_{adj} and Δq and AARE values.

Model stability, i.e., the sensitivity to linearisation and data correction, was assessed by comparing model fits using the (i) nonlinear and linear equations, and (ii) original and corrected data. Additionally, the shift in model parameters (P) was calculated as:

$$Shift(\%) = 100 * \left(\frac{P_{corrected} - P_{orginal}}{P_{orginal}}\right) \quad (31)$$

Beyond numerical fit, we performed an intra-model validation, based on compliance with model assumptions, and an inter-model validation, based on shared assumptions or equivalences (Table 3). Unlike the common approach of selecting the single best-fitting model, our inter-model comparison emphasizes convergence across models, which enhances interpretability of equilibrium conditions, kinetic mechanisms, and isotherm behaviour. This approach allows extracting meaningful insights even from models with lower goodness-of-fit, an aspect often overlooked in prior studies.

2.5. Instruments

Scanning Electron Microscope (SEM) EVO I MA10 Zeiss was used to check the morphology and size of particles. Particle Size distribution was measured using a Malvern Zetasizer Nano ZS Dynamic Light Scattering (DLS) system. This device uses classical single-scattering DLS methods to calculate particle sizes in a range from 0.3 nm to 10 μm with a 633 nm laser and detects the backscattered light at 173°. This device also features a temperature-controlled holder for a cuvette. S measurements were made using a UV-Visible double beam Thermo Fisher Scientific Genesys 30 vis/UV spectrophotometer.

3. Results and discussion

3.1. Preparation of NORDOX suspension

The UV-Visible spectra of NOR suspension in water at varying concentrations and times after preparation are presented in Supplementary Fig. S1. S values increased across the entire wavelength range with increasing NOR concentrations. Minimal spectral shifts were observed after 1 h storage, indicating short-term stability of the suspension. NOR particles in the suspension were further characterised using SEM and DLS (Supplementary Fig. S2A-S2C), confirming a predominant size distribution around 150 nm, which remained stable for at least after 120 min storage.

Unlike dissolved molecules, suspensions lack a standardised protocol for wavelength selection in calibration curves, as the maximum absorption wavelength may shift with concentration. In this case, 490 nm was selected because absorbance at this wavelength showed a minimal slope variation across concentrations and allowed a satisfactory application of Beer's law (Escudey et al., 2025). The concentration of the NOR suspension and calibration curve were determined by gravimetric analysis (Supplementary Fig. S1, Insert).

3.2. Effect of experimental conditions on adsorption data selection

From a practical standpoint, the experimental design required an extended timeframe, therefore the kinetics and adsorption experiments for each experimental data point were conducted on different days. Figs. 2A and 2B present the complete datasets for the kinetic and isotherm adsorption processes, respectively. Selected data points are enclosed by squares.

For adsorption kinetics strong inter-day differences were found without clear trends observed as a function of pH interval ($pH_{NOR\text{-}Metrenco} = 5.53 – 6.11$) or contact time (Fig. 2A).

Strong inter-day differences were observed in adsorption kinetics without clear trends related to pH ($pH_{NOR\text{-}Metrenco} = 5.53 – 6.11$) or contact time (Fig. 2A). Therefore, only kinetic data collected on the same day (day 1) were selected. In contrast, the adsorption isotherm data (Fig. 2B) showed a clear pH-dependent trend ($pH_{NOR\text{-}Metrenco} = [5.50;$

Table 2
Nonlinear and linear model equations to describe adsorption kinetic and isotherm.

Model	References	Nonlinear model		Linear model	
		Equation[a]	Plot[b]	Equation[a]	Plot[b]
Adsorption kinetic models					
Pseudo-second order (PSO)	(Blanchard et al., 1984; Ho and McKay, 1998; Fernández-Bayo et al., 2008; Largitte and Pasquier, 2016; Tran et al., 2017; Vareda, 2023; Azizian, 2004)	$q_t = \frac{q_{eq(PSO)}^2 * k_{2(PSO)} * t}{1 + q_{eq(PSO)} * k_{2(PSO)} * t}$ (7)	q_t vs t	$\frac{t}{q_t} = \left(\frac{1}{q_{eq(PSO)}^2 * k_{2(PSO)}}\right) + \left(\frac{1}{q_{eq(PSO)}}\right) * t$ (8)	t/q_t vs t
Hyperbolic (HYP)	(Fernández-Bayo et al., 2008; Biggar et al., 1978)	$q_t = \left(\frac{q_{eq(HYP)} * t}{B + t}\right)$ (9)	q_t vs t	$\frac{1}{q_t} = \left(\frac{1}{q_{eq(HYP)}}\right) + \left(\frac{B}{q_{eq(HYP)}}\right) * \frac{1}{t}$ (10)	$1/q_t$ vs $1/t$
Elovich (EL)	(Fernández-Bayo et al., 2008; Largitte and Pasquier, 2016; Tran et al., 2017; Vareda, 2023; Zeldowitsch, 1934; Cheung et al., 2000)	$q_t = \frac{1}{\beta_{EL}} * \ln(\alpha_{EL} * \beta_{EL} * t + 1)$ (11)	q_t vs t	$q_t = \frac{1}{\beta_{EL}} * \ln(\alpha_{EL} * \beta_{EL}) + \frac{1}{\beta_{EL}} * \ln(t)$ (12)	q_t vs $\ln(t)$
Dimensionless Elovich (DEL)	(Wu et al., 2009a)	$\left(\frac{q_t}{q_{ref}}\right) = \frac{\ln(\alpha\beta_{DEL} * t + 1)}{\ln(\alpha\beta_{DEL} * t_{ref} + 1)}$ (13)	$\left(\frac{q_t}{q_{ref}}\right)$ vs t	$\left(\frac{q_t}{q_{ref}}\right) = 1 + R_E * \ln\left(\frac{t}{t_{ref}}\right)$ (14)	$\left(\frac{q_t}{q_{ref}}\right)$ vs $\ln\left(\frac{t}{t_{ref}}\right)$
Intraparticle diffusion (IPD)	(Largitte and Pasquier, 2016; Tran et al., 2017; Weber and Morris, 1963; Zhu et al., 2016; Rudzinski and Plazinski, 2007; Wu et al., 2009b)	$q_t = C + k_{int} * \sqrt{t}$ (15)	q_t vs t	$q_t = C + k_{int} * \sqrt{t}$ (16)	q_t vs $\sqrt{t}$
Dimensionless intraparticle diffusion (DIP)	(Wu et al., 2009a, 2009b)	$\left(\frac{q_t}{q_{ref}}\right) = 1 - R_i\left(1 - \sqrt{\frac{t}{t_{ref}}}\right)$ (17)	$\left(\frac{q_t}{q_{ref}}\right)$ vs $\left(\frac{t}{t_{ref}}\right)$	$\left(\frac{q_t}{q_{ref}}\right) = (1 - R_i) + R_i\sqrt{\frac{t}{t_{ref}}}$ (18)	$\left(\frac{q_t}{q_{ref}}\right)$ vs $\sqrt{\frac{t}{t_{ref}}}$
Two-sites non-equilibrium (TSNE)	(Nkedi-Kizza et al., 2006)	$\left(\frac{C_t}{C_0}\right) = \frac{1}{R} + \left(\frac{1}{\beta_{TSNE}R} - \frac{1}{R}\right)\exp^{-\left(\frac{k_{2(TSNE)}}{\beta_{TSNE}}\right)t}$ (19)	$\left(\frac{C_t}{C_0}\right)$ vs t	Not applied	Not applied
		Derived parameters (from Eq. 19):			
		$F = \frac{\beta_{TSNE}R - 1}{R - 1}$ (20)			
		$q_{eq(TSNE)} = \left(\frac{VC_0}{m_{soil}}\right)\left(1 - \frac{1}{R}\right)$ (21)			
		$q_{t=0(TSNE)} = \left(\frac{VC_0}{m_{soil}}\right)\left(1 - \frac{1}{\beta_{TSNE}R}\right)$ (22)			
		$C_{eq(TSNE)} = \left(\frac{C_0}{R}\right)$ (23)			
		$K_{d(TSNE)} = \left(\frac{q_{eq(TSNE)}}{C_{eq}}\right) = (R - 1) * \left(\frac{V}{m_{soil}}\right)$ (24)			
Adsorption isotherm models					
Langmuir	(Tran et al., 2017; Azizian, 2004; Al-Ghouti and Da'ana, 2020)	$q_{eq} = \frac{q_{max} * K_L * C_{eq}}{1 + K_L * C_{eq}}$ (25)	q_{eq} vs C_{eq}	Not applied	Not applied
		Derived parameters (from Eq. 25):			
		$K_{d(Langmuir)} = \left(\frac{q_{eq}}{C_{eq}}\right) = \frac{q_{max} * K_L}{1 + K_L * C_{eq(TSNE)}}$ (26)			
Freundlich	(Tran et al., 2017; Al-Ghouti and Da'ana, 2020)	$q_{eq} = K_F * C_{eq}^{1/n}$ (27)	q_{eq} vs C_{eq}	Not applied	Not applied
		Derived parameters (from Eq. 27):			
		$K_{d(Freundlich)} = \left(\frac{q_{eq}}{C_{eq}}\right) = K_F * C_{eq(TSNE)}^{1/n-1}$ (28)			

[a] $\boldsymbol{1/n}$: Linearity factor (dimensionless). $\boldsymbol{\alpha_{EL}}$: Adsorption rate at t = 0 $\left(mg_{NOR}\ kg_{soil}^{-1}min^{-1}\right)$. $\boldsymbol{\alpha\beta_{DEL}}$: Adsorption rate at t = 0, multiplied by the extent of surface coverage and activation energy for chemisorption (min^{-1}). $\boldsymbol{\beta_{EL}}$: Extent of surface coverage and activation energy for chemisorption $(kg_{soil}mg_{NOR}^{-1})$. $\boldsymbol{\beta_{TSNE}}$: Fraction of retardation for the instantaneous region (dimensionless). $\boldsymbol{B}$: Empirical constant (min). $\boldsymbol{C}$: Thickness of the boundary layer $\left(mg_{NOR}\ kg_{soil}^{-1}\right)$. $\boldsymbol{C_{eq(TSNE)}}$: Aqueous concentration of NOR at the equilibrium condition $(mg_{NOR}\ L^{-1})$. $\boldsymbol{k_{2(PSO)}}$: Second-order adsorption rate constant $\left(mg_{NOR}^{-1}\ kg_{soil}min^{-1}\right)$. $\boldsymbol{k_{2(TSNE)}}$: Kinetic rate coefficient for desorption from time-dependent to instantaneous adsorption sites (min^{-1}). $\boldsymbol{K_{d(Freundlich)}}$, $\boldsymbol{K_{d(Langmuir)}}$ and $\boldsymbol{K_{d(TSNE)}}$: One-point adsorption coefficient at $C_{eq(TSNE)}$ $(L\ kg_{soil}^{-1})$, according to the Freundlich, Langmuir and TSNE model, respectively. One-point adsorption coefficient at $C_{eq(TSNE)}$ $(L\ kg_{soil}^{-1})$. $\boldsymbol{K_F}$: Freundlich adsorption coefficient $\left(mg_{NOR}^{1-1/n}\ kg_{soil}^{-1}\ L^{1/n}\right)$. $\boldsymbol{k_{int}}$: Intraparticle diffusion rate constant $\left(mg_{NOR}kg_{soil}^{-1}\ min^{1/2}\right)$. $\boldsymbol{K_L}$: Langmuir adsorption coefficient (Lmg_{NOR}^{-1}). $\boldsymbol{q_{eq(HYP)}}$, $\boldsymbol{q_{eq(PSO)}}$ and $\boldsymbol{q_{eq(TSNE)}}$: Maximum adsorption capacity of soil at the equilibrium condition according to HYP, PSO and TSNE model, respectively $\left(mg_{NOR}\ kg_{soil}^{-1}\right)$. $\boldsymbol{q_{max}}$:

Maximum adsorption capacity at the saturation of the soil $\left(mg_{NOR}\ kg_{soil}^{-1}\right)$. $\boldsymbol{q_{t=0(TSNE)}}$: Amount of NOR instantaneously adsorbed at t = 0 $\left(mg_{NOR}kg_{soil}^{-1}\right)$. $\boldsymbol{R}$: Retardation factor (dimensionless). $\boldsymbol{R_E}$: Approaching equilibrium factor (dimensionless). $\boldsymbol{R_i}$: Strength of the initial adsorption (dimensionless).

[b] **C_{eq}:** $C_{ads(corr)}$ from Eq. (4) applied to isotherm curves $(mg_{NOR}\ L^{-1})$ at the time closest to equilibrium. **C_t:** $C_{ads(exp)}$ or $C_{ads(corr)}$ from Eqs. (1) and (4) applied to kinetic curves $(mg_{NOR}\ L^{-1})$. **q_{eq}:** $q_{ads(corr)}$ from Eq. (4) applied to isotherm curves $(mg_{NOR}kg_{soil}^{-1})$ at the time closest to equilibrium. **q_{ref}:** Adsorbed amount of NOR at $t = t_{ref}$ $\left(mg_{NOR}kg_{soil}^{-1}\right)$. **$q_t$:** $q_{ads(exp)}$ or $q_{ads(corr)}$ from Eqs. (1) and (4) applied to kinetic curves $(mg_{NOR}kg_{soil}^{-1})$. **t:** Contact time (min). **t_{ref}:** Longest contact time in the adsorption kinetic experiment (min), used as reference.

Table 3
Intra- and inter-model validation applied in this study.

Involved models	Description	Implications
Intra-model validation: Requisites to apply models		
Eq. 12	The shortest contact time, t_{min}, must be much bigger than the inverse multiplication of α_{EL} and β_{EL}.	$t_{min} \gg (\alpha_{EL} * \beta_{EL})^{-1}$
Eq. 13	The longest contact time in the adsorption kinetic experiment (min), t_{ref}, should be equivalent to the t_{ref} value predicted by the DEL model ($t_{ref(pred)}$).	$t_{ref} = t_{ref(pred)}$
Eq. 14	If the intercept is a non-fixed parameter, then it should be near to 1.	Intercept = 1
Eq. 18	The sum of the intercept $(1 - R_i)$ and the slope (R_i) should be near to 1.	Intercept + Slope = 1
Inter-model validation: Equivalences between models		
Eq. 7 and 9	Nonlinear PSO and HYP models are mathematically equivalent.	Same goodness-of-fit (PSO = HYP) $q_{eq(PSO)} = q_{eq(HYP)}$ $\left(q_{eq(PSO)} * k_{2(PSO)}\right)^{-1} = B$
Eq. 11 and 13 Eq. 12 and 14	DEL is originally derived from EL.	$\alpha_{EL} * \beta_{EL} = \alpha\beta_{DEL}$ (Eq. 11and13) $\beta_{EL} = \left(R_E * q_{ref}\right)^{-1}$ (Eq. 12and14)
Eq. 15 and 17; Eq. 16 and 18	DIP is originally derived from IPD. However, to keep the same error structure, the comparisons involve Eq. 15 vs 17, both nonlinear; and Eq. 16 vs 18, both linearised with the same approach (q_t versus $\sqrt{t}$).	$R_i = \left(\frac{k_{int} * \sqrt{t_{ref}}}{q_{ref}}\right)$ (Eq. 15and17; Eq. 16and18)
Inter-model interpretation: Information about the equilibrium condition		
Eq. 7, 9 and 19	Nonlinear PSO, HYP and TSNE predict the adsorbed concentration of NOR at the equilibrium condition.	$q_{eq(PSO)} = q_{eq(HYP)} = q_{eq(TSNE)}$
Eq. 11 and 15	EL and IPD models are only applicable far from equilibrium ($t < t_{eq}$, with Eq. 11 and 15 showing that $q_t \to \infty$ at $t \to \infty$).	Goodness-of-fit = Indicator of equilibrium condition
Eq. 16	If the equilibrium condition is met, then IPD model should exhibit multiple linear regressions when plotting q_t versus $\sqrt{t}$ during the experimental interval of time (Tran et al., 2017; Zhu et al., 2016), where k_{int} regulates the increase of q_t over time, such that each new step has a lower k_{int} value, until $k_{int} \sim 0$ at t_{eq}.	Number of plotted linear regressions = Indicator of equilibrium condition.
Inter-model interpretation: Adsorption kinetic mechanism		
Eq. 11, 15 and 19	EL, IPD and TSNE models assume that adsorption occurs in two steps, firstly a slow one followed by a fast one (Fernández-Bayo et al., 2008; Tran et al., 2017; Zhu et al., 2016; Nkedi-Kizza et al., 2006).	If adsorption is a two-step process: $0 < F < 1$ $0 < C < maximum q_t value$ High goodness-of-fit of EL, IPD and TSNE.
Eq. 15 and 19	If both IPD and TSNE models represent the observed adsorption kinetic behaviour, then both should quantify a similar amount of instantaneous adsorption at t = 0.	$C = q_{t=0(TSNE)}$
Inter-model interpretation: Adsorption isotherm trend		
Eq. 25 and 27	If the experimental adsorption data exhibit a plateau, then the adsorption behaviour fits conceptually better with Langmuir (saturation) than Freundlich, implying a better goodness-of-fit of Langmuir.	If saturation is observed: Goodness-of-fit of Langmuir > Freundlich.
Experimental conditions, Eq. 25 and 27	If the adsorption study was conducted under non-equilibrium conditions, or the adsorption depends on pH, then Langmuir and Freundlich might not fit properly.	If non-equilibrium conditions and/or pH dependence: Potentially low goodness-of-fit of both Langmuir and Freundlich models.
Eq. 19, 25 and 27	If TSNE, Langmuir and Freundlich are able to explain the general adsorption behaviour, then their derived one-point adsorption coefficients quantified at the same C_{eq} value should be similar.	$K_{d(TSNE)} = K_{d(Langmuir)} = K_{d(Freundlich)}$

6.05]), with lower $q_{ads(exp)}$ values at higher $pH_{NOR\text{-}Metrenco}$ when comparing data points at the same C_0 (e.g., ~ 2000, 4000 and 5000 mg L^{-1}). Moreover, $pH_{NOR\text{-}Metrenco}$ was more acidic at C_0 < 4000 mg L^{-1} and more basic at C_0 > 4000 mg L^{-1} (Fig. 2B), indicating that $pH_{NOR\text{-}Metrenco}$ depends on C_0. In fact, a positive correlation between pH_{NOR}, $pH_{NOR\text{-}Metrenco}$ and C_0 was found (Fig. 2C).

Previous studies have reported that the OC% of soils and salt concentration may influence particle suspension stability, thus affecting adsorption process (Baysal et al., 2020; Qi et al., 2014) with OC% closely related to pH. Additionally, C_{soil} is also influenced by OC% and salt content (Sadzawka and Aomine, 1977), but here it showed no strong correlation with pH (Fig. 2D). Further experiments using soils with varying OC content and different ionic strengths are recommended to better understand these effects.

Additionally, NOR stability (f_{sta}) was found to be independent of contact time, C_0 and pH_{NOR} variation (Supplementary Fig. S3A-S3D). Contact time did not affect the pH_{NOR}, which remained higher than $pH_{NOR\text{-}Metrenco}$ (Supplementary Fig. S4A). However, the pH shift from pH_{NOR} to $pH_{NOR\text{-}Metrenco}$, attributed to soil buffering capacity, correlated with both the contact time and C_0 (Supplementary Fig. S4B and S4C), where higher C_0 values corresponded to smaller pH changes. Additionally, C_{soil} was independent of contact time and C_0 (Supplementary Fig. S5A and S5B).

Based on this analysis, data selection proceeded in two steps. First, stability criteria involving f_{sta} and f_{var} (2.3.2) were applied. Then, kinetic data with normally distributed pH values were accepted

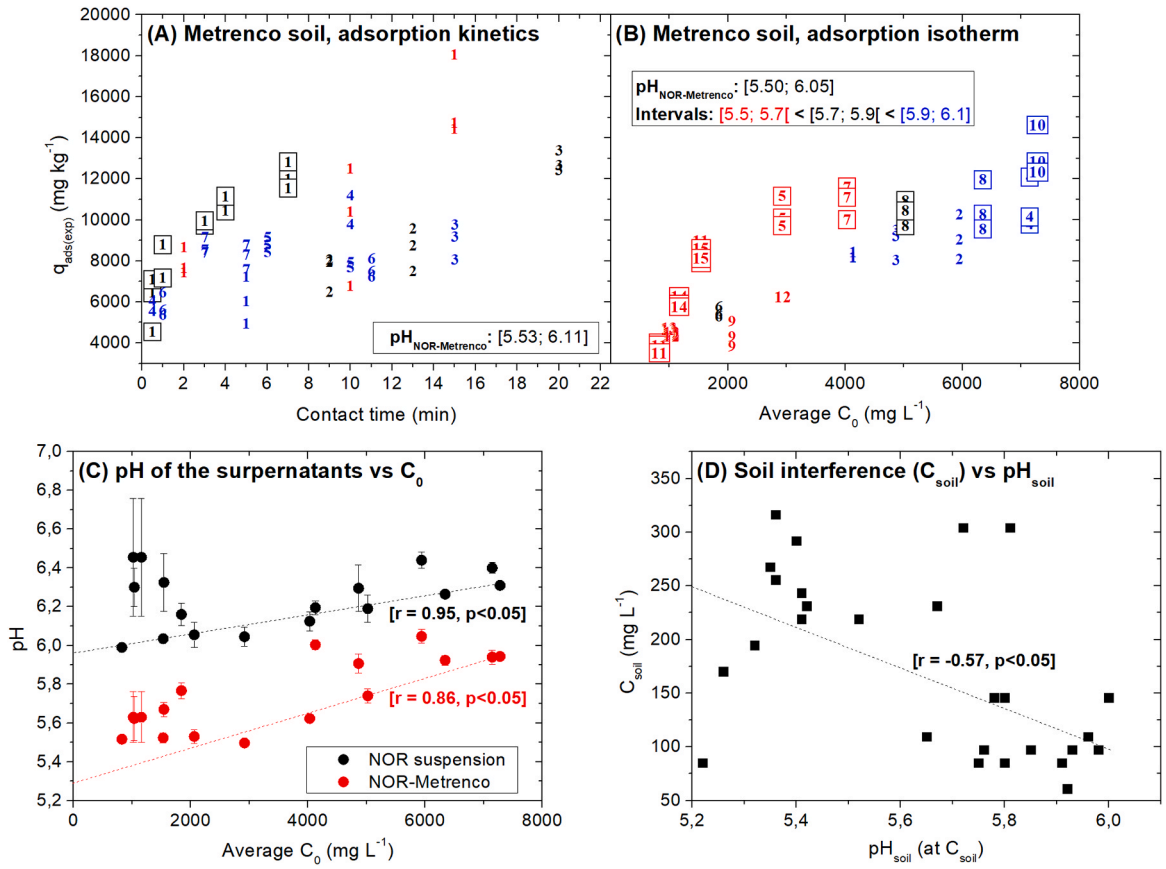

Fig. 2. Total experimental data obtained during the **(A)** adsorption kinetics (7 days) and **(B)** adsorption isotherm studies (15 days) on Metrenco soil, where numbers show the day of experimental work, colours represent pH ranges, and square-enclosed points are comparable experimental data used for modelling in 3.3. Effect of **(C)** initial concentration of NOR (C_0) on pH, and **(D)** pH_{soil} on soil interference (C_{soil} from kinetics and adsorption isotherm studies), where r and p represent the Pearson correlation coefficients derived from correlation analyses and p-value (significance level was set on 0.05), respectively.

(Supplementary Fig. S6A), as they are expected to reflect consistent C_0 and pH values. Also, isotherm data that followed the empirical pH trend where $pH_{NOR-Metrenco}$ increases with C_0 but not necessarily linearly, as observed near $C_0 \sim 2000$ L^{-1} (Supplementary Fig. S6B and Fig. 2C), were retained.

3.3. Adsorption kinetics modelling

Nonlinear PSO, HYP, EL, IPD and TSNE model fittings using the selected data are shown in Fig. 3. The remaining linear and nonlinear kinetic model fittings are presented in Supplementary Fig. S7 and S8, respectively.

The average C_0 value for the selected data points was 4000 $\pm$ 160 mg_{NOR} L^{-1}. The contact time for the kinetic study ranged from 0.5 to 7 min. The maximum experimental concentration observed for NOR, max(q_t), was 11800 $\pm$ 300 $mg_{NOR}kg_{soil}^{-1}$ for the original data and 11900 $\pm$ 300 $mg_{NOR}kg_{soil}^{-1}$ for the corrected data, representing about 5 % increase after correction. The benefits of this correction are observed on the improvement of model fits.

Mathematical equation, statistical quality and model parameters (mean value $\pm$ standard deviation) for the nonlinear PSO, HYP, EL, IPD and TSNE models fitted to both the original and corrected kinetic data are summarised in Table 4. Linearised and dimensionless models are provided in Supplementary Tables S1 and S2, respectively.

3.4. Data correction and stability of models

Data correction resulted in noticeable shifts in the calculated model parameters compared to the original data (PSO, EL and IPD models, Table 4). Excluding the IPD model, the largest changes occurred in kinetic parameters associated with NOR transport, such as $k_{2(PSO)}$ (+12.2 %), B (-9.8 %) and α_{EL} (+24.4 %). In contrast, parameters related to the soil adsorption capacity and affinity, such as $q_{eq(PSO)}$ (-1.1 %), $q_{eq(HYP)}$ (-1.1 %) and β_{EL} (+4.9 %), were less affected. These results suggest that bulk-adsorbent parameters are less sensitive to data correction than transport-related parameters, indicating that the correction primarily impacts NOR-specific processes without altering the overall conceptual meaning of parameters.

Additionally, TSNE model uses the C_t/C_0 ratio as response variable, with both C_t and C_0 scaled by $f^*_{sta} * f_{var}$. Therefore, TSNE parameters remained unchanged after data correction, making it the most stable model. On the other hand, EL and DEL models exhibited the largest shifts, indicating lower stability

In terms of goodness-of-fit, data correction improved the fitting for the IPD model (R^2_{adj}, Δq and AARE), while worsened the adjustment of PSO (only R^2_{adj}), and increased some of the standard deviation for some calculated parameters. Nevertheless, R^2_{adj} and AARE values did not significantly vary after data correction for the EL and TSNE models, while variations in Δq are related to changes in the magnitude of data. Assuming that the correction enhances the representational value of the data by the consideration of NOR instability, then the changes in goodness-of-fit values should be interpreted as the sensitivity of models to produce false positives or negatives when corrections are not considered, i.e., if the model fit was overestimated or underestimated, respectively, producing interpretation biases when selected to interpret results.

In addition, the use of linear versions of some kinetic models might

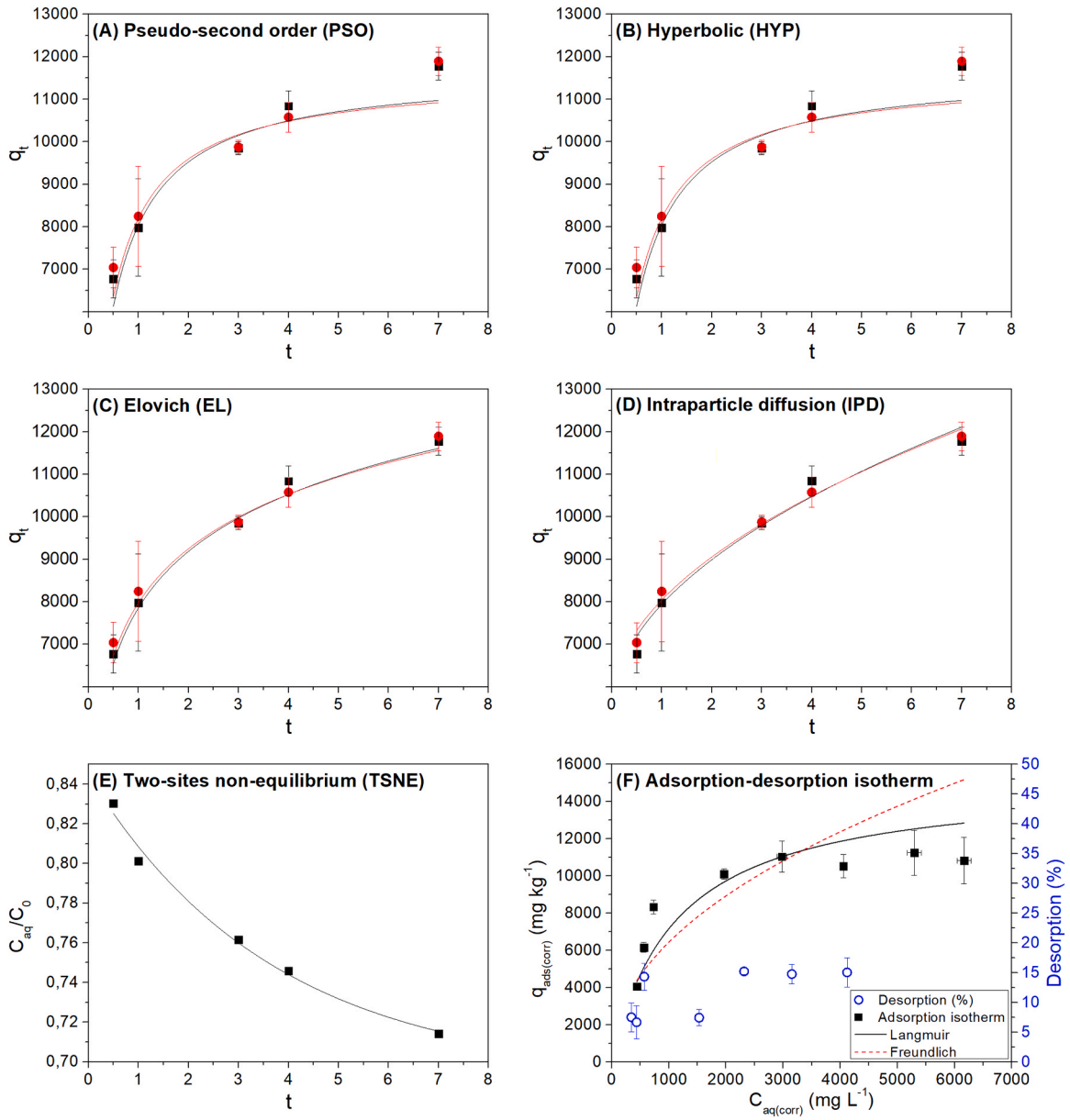

Fig. 3. Nonlinear (A) Pseudo-second order, (B) Hyperbolic, (C) Elovich, (D) Intraparticle diffusion and (E) Two-sites non-equilibrium models fitted to the original (black data and trendline) and corrected (red data and trendline) kinetic experimental data. (F) Adsorption isotherm (black solid) and desorption percentage (blue hollow) trends for Metrenco soil. Trendlines represent the Langmuir (solid black) and Freundlich (dash red) model fitted to the corrected experimental data.

produce distortion of the statistical assumption (Chowdhury and Saha, 2011; El-Khaiary et al., 2010), hence biases, during the interpretation of results. This potential bias was tested by comparing goodness-of-fit and parameters between nonlinear (Table 4) and linear model equations (Supplementary Table S1). Variability in parameters depended more on linearisation than on data correction, with PSO ($k_{2(PSO)}$, Eq. 7 versus 8) and HYP (B, Eq. 9 versus 10) presenting the higher changes. Additionally, differences between linear and nonlinear fittings were found for PSO and HYP ($R^2_{adj(linear)} > R^2_{adj(nonlinear)}$ but $AARE_{(linear)} > AARE_{(nonlinear)}$), implying that linearisation has a large impact in the interpretation of models. This situation has been previously reported for PSO model and associated to the response variable in Eq. 8, which is a relationship between X and Y axis of Eq. 7 (t/q_t), producing two problems (El-Khaiary et al., 2010): First, the higher the q_t values, the lower the relative weights of data, creating an inverse trend of relative weights between Eq. 7 and 8 (q_t and $1/q_t$). Second, the presence of the same variable (t) in both X and Y axis in Eq. 8 induces an artificial dependence between X and Y, promoting spurious correlations and overestimating R^2_{adj}. In this sense, an unreliable fit is expected when most of the data are close to the equilibrium condition (Revellame et al., 2020), while AARE becomes a better descriptor for goodness-of-fit.

From the observations made, it seems that the direct use of experimental data in some cases provokes relatively important parameter underestimation of kinetic adsorption models on a full complex soil sample. On the other hand, corrected data enable a better mechanical interpretation of experimental outcomes in terms of reliability of the model interpretation. Thus, on the subsequent parts of the present work the observation would be made solely on corrected data outcomes.

3.5. Intra-model validation

The intra-model validation is shown in Supplementary Table S1 and S2. For EL model (Eq. 12), we found that t_{min} and $(\alpha_{EL} * \beta_{EL})^{-1}$ were 0.5 and 0.010 $\pm$ 0.002 min, respectively. On the case of DEL fitting of data, the empirical and predicted t_{ref} for Eq. 13 were 7 and 8.0 $\pm$ 0.8 min,

Table 4
Model parameters and goodness-of-fit obtained by using the original and corrected experimental data to fit nonlinear adsorption kinetics and isotherm models.

	Parameters	Original	Corrected	Shift (%)
Pseudo-second order (PSO) (Eq. 7)				
Model parameters[a]	$q_{eq(PSO)}$ $\left(mg_{NOR}kg_{soil}^{-1}\right)$	11700 ± 600	11600 ± 700	−1.1
	$k_{2(PSO)}$ $\left(mg_{NOR}^{-1}\ kg_{soil}min^{-1}\right)$	(1.9 ± 0.8) x10^{-4}	(2.1 ± 1.0) x10^{-4}	+ 12.2
Goodness-of-fit	R_{adj}^2	0.81	0.75	-
	$\Delta q\ \left(mg_{NOR}kg_{soil}^{-1}\right)$	3428	3905	-
	AARE(%)	4.67	4.46	-
Inter-validation[2]	$\left(q_{eq(PSO)} * k_{2(PSO)}\right)^{-1}$ (min)	0.5 ± 0.2	0.4 ± 0.2	-
Hyperbolic (HYP) (Eq. 9)				
Model parameters	$q_{eq(HYP)}$ $\left(mg_{NOR}kg_{soil}^{-1}\right)$	11700 ± 600	11600 ± 700	−1.1
	B(min)	0.45 ± 0.17	0.41 ± 0.17	−9.8
Goodness-of-fit	R_{adj}^2	0.81	0.75	-
	$\Delta q\ \left(mg_{NOR}kg_{soil}^{-1}\right)$	3428	3908	-
	AARE(%)	4.67	4.46	-
Elovich (EL) (Eq. 11)				
Model parameters	α_{EL} $\left(mg_{NOR}\ kg_{soil}^{-1}min^{-1}\right)$	(1.1 ± 0.4) x10^{5}	(1.4 ± 0.6) x10^{5}	+ 24.4
	β_{EL} $\left(kg_{soil}mg_{NOR}^{-1}\right)$	(5.1 ± 0.5) x10^{-4}	(5.4 ± 0.6) x10^{-4}	+ 4.9
Goodness-of-fit	R_{adj}^2	0.97	0.96	-
	$\Delta q\ \left(mg_{NOR}kg_{soil}^{-1}\right)$	568	866	-
	AARE(%)	2.10	2.47	-
Inter-validation	$\alpha_{EL} * \beta_{EL}$ $\left(min^{-1}\right)$	60 ± 20	70 ± 30	-
Intraparticle diffusion (IPD) (Eq. 15)				
Model parameters	$C(mg_{NOR}\ kg_{soil}^{-1})$	5400 ± 500	5600 ± 300	+ 3.6
	$k_{int}\left(mg_{NOR}kg_{soil}^{-1}\ \ min^{-1/2}\right)$	2500 ± 300	2400 ± 150	−3.5
Goodness-of-fit	R_{adj}^2	0.96	0.99	-
	$\Delta q\ \left(mg_{NOR}kg_{soil}^{-1}\right)$	1226	500	-
	AARE(%)	2.71	1.86	-
Two-sites non-equilibrium (TSNE) (Eq. 19; same fit for original and corrected data)				
Model parameters	R	1.44 ± 0.04	1.44 ± 0.04	0
	β_{TSNE}	0.82 ± 0.03	0.82 ± 0.03	0
	$k_{2(TSNE)}$ $\left(min^{-1}\right)$	0.22 ± 0.07	0.22 ± 0.07	0
Derived parameters	F	0.41 ± 0.04	0.41 ± 0.04	0
	$q_{t=0(TSNE)}$ $\left(mg_{NOR}kg_{soil}^{-1}\right)$	6300 ± 400	6300 ± 400	0
	$C_{eq(TSNE)}$ $\left(mg_{NOR}\ L^{-1}\right)$	2790 ± 140	2790 ± 140	0
	$q_{eq(TSNE)}$ $\left(mg_{NOR}\ kg_{soil}^{-1}\right)$	12000 ± 1000	12000 ± 1000	0
	$K_{d(TSNE)}$ $\left(L\ kg_{soil}^{-1}\right)$	4.4 ± 0.4	4.4 ± 0.4	0
Goodness-of-fit	R_{adj}^2	0.98	0.98	-
	AARE(%)	0.43	0.43	-
Langmuir (Eq. 25)				
Model parameters	q_{max} $\left(mg_{NOR}\ kg_{soil}^{-1}\right)$	-	15000 ± 2000	-
	K_L $\left(Lmg_{NOR}^{-1}\right)$	-	(9 ± 2) x10^{-4}	-
Derived parameters	$K_{d(Langmuir)}$ $\left(Lmg_{NOR}^{-1}\right)$	-	3.9 ± 0.6	-
Goodness-of-fit	R_{adj}^2	-	0.88	-
	$\Delta q\ \left(mg_{NOR}kg_{soil}^{-1}\right)$	-	22434	-
	AARE(%)	-	12.37	-
Freundlich (Eq. 27)				
Model parameters	K_F $\left(mg_{NOR}^{1-1/n}\ \ kg_{soil}^{-1}mL^{1/n}\right)$	-	250 ± 130	-
	1/n	-	0.47 ± 0.07	-
Derived parameters	$K_{d(Freundlich)}$ $\left(Lmg_{NOR}^{-1}\right)$	-	4 ± 3	-
Goodness-of-fit	R_{adj}^2	-	0.78	-
	$\Delta q\ \left(mg_{NOR}kg_{soil}^{-1}\right)$	-	59915	-
	AARE(%)	-	20.05	-

[a] Model parameters and derived parameters are described in Table 2. Inter-validation equations are shown in Table 3.

respectively. Additionally, the intercept of Eq. 14 was near to 1 (0.98 ± 0.01). For linear DIP fitting of data, Eq. 18, intercept + slope was near to 1 (1.01 ± 0.05). In this sense, EL, DEL and DIP met the requirements to be used during the interpretation of adsorption mechanisms (Table 3).

3.6. Inter-model validation

We corroborated the equivalence between nonlinear PSO and HYP models (Eq. 7 and 9), both sharing the same goodness-of-fit, with $q_{eq(PSO)} = q_{eq(HYP)}$ and identical values of $\left(q_{eq(PSO)} * k_{2(PSO)}\right)^{-1}$ and B (0.4 ± 0.2 min). However, their different assumptions make them complementary models. For example, HYP was proposed to describe the adsorption of pesticides on soils using a flow technique (Biggar et al., 1978), where parameter B is conceptually related to solute transport on columns. Therefore, if the interpretation for column and batch studies does not change significantly, then $k_{2(PSO)}$ is also linked to solute transport.

Although the comparison between $\alpha_{EL} * \beta_{EL}$ (Eq. 11) and $\alpha\beta_{DEL}$ (Eq. 13) is imprecise due to the high standard deviation, there is a partial overlap between both parameters (70 ± 30 vs 100 ± 30 min^{-1}),

implying EL and DEL models are similar. Additionally, parameters β_{EL} (Supplementary Table S1, Eq. 12) and $\left(R_E * q_{ref}\right)^{-1}$ (Supplementary Table S2, Eq. 14) of linear EL and DEL models had identical value of ($(5.6 \pm 0.4) \times 10^{-4}$ $kg_{soil}mg_{NOR}^{-1}$). AARE values of nonlinear EL and DEL were also identical.

Finally, R_i parameter in DIP (Supplementary Table S2, Eq. 17 and 18) was compared to $\left(k_{int} * \sqrt{t_{ref}}/q_{ref}\right)$ in IPD, obtaining identical values only for linearised models (0.54 ± 0.04), while for nonlinear models we found slight differences (0.522 ± 0.018 vs 0.54 ± 0.04). IPD and DIP models had the same AARE values.

3.7. Inter-model interpretation

Finally, the results were interpreted considering only the nonlinear equations because they share the same axis (q_t vs t), producing equivalent, unaltered and comparable error structures (Chowdhury and Saha, 2011; El-Khaiary et al., 2010).

3.7.1. Equilibrium condition

For NOR adsorbed on Metrenco soil, the $q_{eq(PSO)}$ and $q_{eq(TSNE)}$ values were 11600 ± 700 and 12000 ± 1000 $mg_{NOR}kg_{soil}^{-1}$, respectively, both close to the maximum empirical q_t (11900 ± 300 $mg_{NOR}kg_{soil}^{-1}$), though with a high standard deviation. Due to the lower standard deviation of $C_{eq(TSNE)}$, it was used to assess the equilibrium condition. The empirical C_{aq} (Eq. 1) at the longest contact time was (3230 ± 40) mg_{NOR} L^{-1} for the corrected data, 16 % higher than $C_{eq(TSNE)}$, indicating a non-equilibrium condition.

In addition, the EL, IPD and TSNE models showed a better fit (R^2_{adj} = 0.96 – 0.99; AARE = 0.43 – 2.47; Δq = 500 – 866 $mg_{NOR}kg_{soil}^{-1}$) that the PSO and HYP models (R^2_{adj} = 0.75; AARE = 4.46; Δq = 3905), supporting the presence of a non-equilibrium condition (see Table 3). This is further supported by the IPD model plot, which showed only one diffusion step with $k_{int} > 0$ (Supplementary Fig. S7E).

3.7.2. Adsorption kinetic mechanisms

A two-step adsorption kinetics is evidenced by the TSNE ($0 < F < 1$) and IPD ($0 < C <$ maximum q_t value) models (Table 4). Additionally, the similar goodness-of-fit for EL, IPD and TSNE suggest that this two-step assumption is central to their framework, independent of the other model-specific assumptions.

Specifically, the slow step is associated with non-specific solute transport in EL model (Fernández-Bayo et al., 2008; Tran et al., 2017), and with diffusion in the IPD model (Zhu et al., 2016). This comparison indicates that the EL model provides a less detailed description of the transport than the IPD model. Therefore, a good fit of both models in Metrenco soil suggest that solute transport is primarily diffusion-driven.

At the beginning of the experiment, Metrenco soil had no detectable NOR (C_{aq} and $C_{ads} = 0$ at $t = 0$). However, both the IPD and TSNE models yielded $q_t > 0$ at $t = 0$. This can be attributed to two possible explanations: (i) the presence of instantaneous adsorption sites, as conceptualised by the TSNE model (Nkedi-Kizza et al., 2006), or (ii) adsorption occurring so rapidly that it was not detected experimentally, as implied by the IPD model (Zhu et al., 2016). Both interpretations are consistent with our results. NOR adsorption was notably fast (kinetic study conducted at $t \leq 7$ min), and shorter contact times led to higher experimental uncertainty. Similar findings have been reported in the literature. For example, zero valence iron particles showed rapid adsorption onto the inorganic fraction of volcanic soils (Gacitua et al., 2022). Likewise, Khepar et al. (2024) (Khepar et al., 2024) found that ZnS nanoparticles adsorb more quickly than free Zn^{+2} ions in an agricultural loamy sand soil (1.8 % OC, pH 5.83). These observations suggest that, regardless of the adsorbent, particle-based adsorbates may undergo faster adsorption compared to dissolved, homogeneous species. However, further studies are necessary to generalise this behaviour across systems.

Finally, the values of C (IPD) and $q_{t=0(TSNE)}$ were similar (Table 4), suggesting that both models accurately represent the NOR-Metrenco adsorption behaviour. Therefore, instantaneous adsorption and methodological issues could explain the initial NOR adsorption observed in the studied soils. The impact of this proposal was assessed by comparing the goodness-of-fit of the PSO model (Eq. 7) with a modified PSO model (MPSO). For MPSO, it was assumed that $q_t = 0$ at $t = 0$ but instantaneous adsorption and/or methodological issues occurred, such that $q_{t=0} > 0$. Thus, after integrating the PSO kinetic rate equation with the boundary condition $\lim_{t\to 0} q_t$ or $q_{t=0} > 0$ at $t = 0$, the following equation was obtained:

$$q_t = \left(\frac{q_{eq(MPSO)}\left(q_{eq(MPSO)}k_{2(MPSO)}t + \delta_{MPSO} - 1\right)}{q_{eq(MPSO)}k_{2(MPSO)}t + \delta_{MPSO}} \right) \quad (32)$$

Where $\delta_{MPSO} = q_{eq(MPSO)}/\left(q_{eq(MPSO)} - q_{t=0(MPSO)}\right)$ is a measure of the deviation from the original PSO model, such that Eq. 32 becomes the Eq. 7 when $\delta_{MPSO} = 1$ ($q_{t=0} = 0$). Additionally, $q_{t=0(MPSO)}$ can be quantified through the equation:

$$q_{t=0(MPSO)} = q_{eq(MPSO)}\left(1 - \frac{1}{\delta_{MPSO}}\right) \quad (33)$$

The goodness-of-fit (corrected data) improved 33 % (R^2_{adj} from 0.75 to 0.997, Δq from 3905 to 518 $mg_{NOR}kg_{soil}^{-1}$, AARE from 4.46 to 1.16), with $\delta_{MPSO} = 1.64 \pm 0.03$. Moreover, a $q_{eq(MPSO)}$ value of 15800 ± 600 $mg_{NOR}kg_{soil}^{-1}$ was obtained, implying a non-equilibrium condition as suggested by EL, IPD and TSNE models. Finally, $q_{t=0(MPSO)}$ was 6200 ± 200 $mg_{NOR}kg_{soil}^{-1}$, similar to $q_{t=0(TSNE)}$ and C values derived from IPD model (Table 4), contributing to the interpretation of instantaneous adsorption and methodological issues as indistinguishable situations.

3.7.3. Adsorption isotherm

Selected data for the isotherm experiments and model fittings (Freundlich and Langmuir) are shown in Fig. 3F. Experimentally, the maximum adsorbed NOR concentration reached after the isothermal adsorption process was $11000 + 1300$ $mg_{NOR}kg_{soil}^{-1}$. This value is close to the maximum q_t calculated from the corrected kinetic data set (11900 ± 300 $mg_{NOR}kg_{soil}^{-1}$), meaning that the Metrenco soil reached its maximum adsorption capacity during the kinetic study.

Mathematical equation, statistical quality and parameters (mean value $\pm$ standard deviation) for the models fitted to isothermal selected data sets are summarised in Table 4.

The Langmuir model is based on several assumptions, including a homogeneous adsorption surface (Tran et al., 2017; Al-Ghouti and Da'ana, 2020). Despite this, Eq. 25 has been successfully applied to describe adsorption on soils, which are inherently complex and heterogeneous (Al-Ghouti and Da'ana, 2020). In contrast, the Freundlich model is empirical (Tran et al., 2017; Al-Ghouti and Da'ana, 2020). Therefore, Eq. 25 and 27 were compared in this study without assuming a mechanistic explanation.

Conceptually, Eq. 25 (Langmuir) describes adsorption across a wide range of C_{eq}, from linear behaviour at low concentrations ($1 \gg K_L C_{eq}$) to saturation at high concentrations ($1 \ll K_L C_{eq}$). In contrast, Eq. 27 (Freundlich) can resemble the Langmuir shape when $1/n < 1$, but the parameter $1/n$ is highly dependent on the experimental C_{eq} range. At low C_{eq}, adsorption tends to be linear, leading to $1/n \approx 1$. At high C_{eq}, where more data points approach saturation ($q_{eq} = q_{max}$), $1/n$ approaches zero to reflect the independence of q_{eq} from C_{eq}. Therefore, Eq. 27 is best suited for narrower C_{eq} intervals in systems that are either (i) far from saturation ($1/n < 1$) (Tran et al., 2017), or (ii) involve multilayer adsorption without saturation ($1/n > 1$) (Al-Ghouti and Da'ana,

2020).

The adsorption isotherms covered a wide range of C_{eq}, with NOR adsorption on Metrenco soil approaching saturation around 3000 mg/L (Fig. 3F), which explains the better fit of Langmuir compared to the Freundlich model. In contrast, (Julich and Gäth, 2014) found that CuO nanoparticle adsorption on agricultural soils from Hesse, Germany, was better described by the Freundlich model. Their study differed in several ways: they used different soils and compared free Cu^{2+} with water-suspended CuO nanoparticles, rather than a Cu_2O nanopesticide formulation like NOR. Still, they concluded that copper oxide nanoparticles are more strongly adsorbed than free copper, a trend that aligns with Khepar et al. (2024) (Khepar et al., 2024), who found a similar behaviour for ZnS versus Zn^{+2}, as well as with the rapid adsorption of NOR on Metrenco soil observed in this study. However, Julich applied the linear form of the Freundlich equation, which, as discussed for kinetic models, can influence interpretation. Overall, comparisons across studies require attention not only to experimental conditions (e.g., solutes, adsorbents, procedures) but also to how thoroughly the modelling and interpretation were performed.

The Langmuir model assumes an equilibrium condition, where $t \rightarrow t_{eq}$ and $q_t \rightarrow q_{eq}$ (Azizian, 2004). In our study, a contact time of 7 min was chosen to minimize potential bias from NOR instability during the isotherm experiments. However, this short duration likely resulted in a non-equilibrium state, affecting the isotherm shape and violating the assumptions of the Langmuir model. Furthermore, the effect of pH on C_0 (Fig. 2A) leads to a pH-dependent adsorption trend that is not accounted for by the adsorption isotherm models. The combined effects of non-equilibrium condition and pH-dependent adsorption may explain the low goodness-of-fit observed for both the Langmuir and Freundlich models in Metrenco soil.

To connect adsorption kinetics with isotherm studies, further calculations were considered using PSO and TSNE modelling outcomes.

The interpretation of PSO model varies in the literature: (i) as irreversible adsorption, where solute concentration changes minimally at the start, making the rate dependent on the availability of two adsorption sites (Blanchard et al., 1984; Fernández-Bayo et al., 2008; Largitte and Pasquier, 2016; Vareda, 2023); or (ii) as reversible adsorption involving one solute molecule and one adsorption site (Azizian, 2004). The desorption results in Fig. 3F indicate that the process was reversible, rejecting the first interpretation. However, the second interpretation assumes the condition $C_0 \gg (m_{soil}/V)q_t$ is not satisfied (Vareda, 2023; Azizian, 2004). In our study, $(m_{soil}/V)q_t$ ranged from 680 $\pm$ 40–1180 $\pm$ 30 $mg_{NOR}L^{-1}$, representing 17 – 30 % of the average C_0 used in the kinetic experiments. This partial violation of the assumption may help explain the low goodness-of-fit observed in the nonlinear PSO model fits (Table 4).

On the other hand, the K_d values obtained from the Langmuir and Freundlich models were close to $K_{d(TSNE)}$ (Table 4). Based on the interpretations of the PSO, EL, IPD, and TSNE models, and considering the standard deviations of $K_{d(Langmuir)}$ and $K_{d(Freundlich)}$, the adsorption kinetic study was likely conducted near, but not at, equilibrium. This may account for the discrepancies among the K_d values. Moreover, the similarity between $K_{d(Langmuir)}$ and $K_{d(Freundlich)}$ suggests that both models represent the system equally well at the selected C_{eq}.

4. Conclusion

The NOR-soil system demonstrated complex adsorption behaviour, where both data treatment and model assumptions significantly influenced the interpretation of results. This highlights the need for structured, transparent procedures in both the production and analysis of adsorption data, especially when such data help regulatory decisions.

To address these challenges, we propose a two-step framework designed to minimise bias and enhance interpretability in studies of nanomaterial adsorption. First, during data production, experimental conditions should be selected based on methodological (e.g., experiment duration, interval of C_0) and contextual (e.g., pH, NOR stability) variables that influence system comparability. Second, data interpretation should avoid a single best-fit model selection based on R^2_{adj} alone. Instead, it should incorporate a set of statistically comparable models (e.g., sharing the same error structure) with diverse assumptions, using both good and poor fits to reveal mechanistic insights.

This multi-model strategy shifts the focus from merely fitting data to understanding the processes behind them. It allowed us, for example, to formulate a modified PSO model that not only improved statistical performance but also aligned with mechanistic patterns observed across IPD, EL, and TSNE models. This procedure offers a more robust, evidence-based foundation for evaluating adsorption dynamics in complex environmental systems

CRediT authorship contribution statement

Neira Albornoz Angelo: Visualization, Validation, Methodology, Writing – review & editing, Writing – original draft, Formal analysis, Data curation, Conceptualization. **Manuel Gacitua:** Writing – review & editing, Writing – original draft, Visualization, Validation, Resources, Project administration, Methodology, Investigation, Funding acquisition, Formal analysis, Conceptualization.

Funding

This work was supported by Basal Funding for Scientific and Technological Centers of Excellence, CEDENNA [AFB220001 and CIA250002], and the Federal Ministry of Education and Research (BMBF) and the Baden-Württemberg Ministry of Science as part of the Excellence Strategy of the German Federal and State Governments. We gratefully acknowledge the University of Konstanz for partial funding the open-access publication of this work. Manuel Gacitua thanks FONDECYT [grant #1220272]. Angelo Neira-Albornoz was supported by the 2-year Postdoctoral Fellowship of the Zukunftskolleg, University of Konstanz.

Declaration of Competing Interest

The authors declare that they have no known competing financial interests or personal relationships that could have appeared to influence the work reported in this paper.

Appendix A. Supporting information

Supplementary data associated with this article can be found in the online version at doi:10.1016/j.ecoenv.2025.119075.

Data availability

Data will be made available on request.

References

Al-Ghouti, M.A., Da'ana, D.A., 2020. Guidelines for the use and interpretation of adsorption isotherm models: a review. J. Hazard. Mater. 393, 122383. https://doi.org/10.1016/j.jhazmat.2020.122383.

Azizian, S., 2004. Kinetic models of sorption: a theoretical analysis. J. Colloid Interface Sci. 276 (1), 47–52. https://doi.org/10.1016/j.jcis.2004.03.048.

Báez, M.E., et al., 2015. Sorption-desorption behavior of pesticides and their degradation products in volcanic and nonvolcanic soils: interpretation of interactions through two-way principal component analysis. Environ. Sci. Pollut. Res. 22 (11), 8576–8585. https://doi.org/10.1007/s11356-014-4036-8.

Baysal, A., Saygin, H., Ustabasi, G.S., 2020. Risks of graphene nanomaterial contamination in the soil: evaluation of major ions. Environ. Monit. Assess. 192 (10), 622. https://doi.org/10.1007/s10661-020-08561-2.

Besoain, E., 1985. In: Tosso, J. (Ed.), Mineralogía de los suelos volcánicos del centro-sur de Chile, in Suelos Volcánicos de Chile. INIA, Chile.

Biggar, J.W., Mingelgrin, U., Cheung, M.W., 1978. Equilibrium and kinetics of adsorption of picloram and parathion with soils. J. Agric. Food Chem. 26 (6), 1306–1312. https://doi.org/10.1021/jf60220a009.

Blanchard, G., Maunaye, M., Martin, G., 1984. Removal of heavy metals from waters by means of natural zeolites. Water Res. 18 (12), 1501–1507. https://doi.org/10.1016/0043-1354(84)90124-6.

Burachevskaya, M., et al., 2021. Transformation of copper oxide and copper oxide nanoparticles in the soil and their accumulation by hordeum sativum. Environ. Geochem. Health 43 (4), 1655–1672. https://doi.org/10.1007/s10653-021-00857-7.

Cáceres, L., et al., 2010a. Metsulfuron-methyl sorption/desorption behavior on volcanic ash-derived soils. Effect of phosphate and ph. J. Agric. Food Chem. 58 (11), 6864–6869. https://doi.org/10.1021/jf904191z.

Cáceres, L., et al., 2010b. Modeling the sorption kinetic of metsulfuron-methyl on andisols and ultisols volcanic ash-derived soils: kinetics parameters and solute transport mechanisms. J. Hazard. Mater. 179 (1), 795–803. https://doi.org/10.1016/j.jhazmat.2010.03.074.

Caceres-Jensen, L., et al., 2019. Electrochemical method to study the environmental behavior of glyphosate on volcanic soils: proposal of adsorption-desorption and transport mechanisms. J. Hazard. Mater. 379, 120746. https://doi.org/10.1016/j.jhazmat.2019.120746.

Cáceres-Jensen, L., et al., 2013. Sorption kinetics of diuron on volcanic ash derived soils. J. Hazard. Mater. 261, 602–613. https://doi.org/10.1016/j.jhazmat.2013.07.073.

Cheung, C.W., Porter, J.F., McKay, G., 2000. Elovich equation and modified second-order equation for sorption of cadmium ions onto bone char. J. Chem. Technol. Biotechnol. 75 (11), 963–970. https://doi.org/10.1002/1097-4660(200011)75:11<963::AID-JCTB302>3.0.CO;2-Z.

Chowdhury, S., Saha, P., 2011. Pseudo-second-order kinetic models for the sorption of malachite Green onto tamarindus indica seeds: comparison of linear and non-linear methods. Desalin. Water Treat. 30 (1), 1–8. https://doi.org/10.5004/dwt.2011.2044.

El-Khaiary, M.I., Malash, G.F., Ho, Y.-S., 2010. On the use of linearized pseudo-second-order kinetic equations for modeling adsorption systems. Desalination 257 (1), 93–101. https://doi.org/10.1016/j.desal.2010.02.041.

Escudey, M., Cáceres-Jensen, L., Gacitúa, M., 2025. Determination of particle mixture composition by visible spectroscopy. Colloids Interfaces 9. https://doi.org/10.3390/colloids9020016.

Fernández-Bayo, J.D., Nogales, R., Romero, E., 2008. Evaluation of the sorption process for imidacloprid and diuron in eight agricultural soils from Southern Europe using various kinetic models. J. Agric. Food Chem. 56 (13), 5266–5272. https://doi.org/10.1021/jf8004349.

Fortune-Business-Insights. *Nanotechnology market size, share & industry analysis, by type (nanodevices and nanosensors), by industry (electronics, healthcare, manufacturing, energy & power, automotive, aerospace & defense, food & beverages, and others), and regional forecast, 2024 – 2032. 2024* [Accessed: 2024 June, 20th]; Available from: ⟨https://www.fortunebusinessinsights.com/nanotechnology-market-108466⟩.

Gacitua, M., et al., 2022. Adsorption of zerovalent iron nanoparticles in the inorganic fraction of volcanic soils. J. Soil Sci. Plant Nutr. 22 (2), 2392–2405. https://doi.org/10.1007/s42729-022-00816-w.

Ho, Y.S., McKay, G., 1998. Sorption of dye from aqueous solution by peat. Chem. Eng. J. 70 (2), 115–124. https://doi.org/10.1016/S0923-0467(98)00076-1.

Hunter, R.J., 1981. Zeta Potential in Colloid Science: Principles and Applications. Academic Press, London.

Julich, D., Gäth, S., 2014. Sorption behavior of copper nanoparticles in soils compared to copper ions. Geoderma 235-236, 127–132. https://doi.org/10.1016/j.geoderma.2014.07.003.

Khepar, V., Sidhu, A., Chandel, S., 2024. Sustained release of zn from zinc sulfide nanoparticles (ZnS NPs) amplified the bioaccessibility of zn in soil: adsorption dynamics and dissolution kinetics. Environ. Res. 251, 118624. https://doi.org/10.1016/j.envres.2024.118624.

Kiaune, L., Singhasemanon, N., 2011. Pesticidal copper (I) oxide: environmental fate and aquatic toxicity. In: Whitacre, D.M. (Ed.), Reviews of Environmental Contamination and Toxicology Vol. 213. Springer New York, New York, NY, pp. 1–26. https://doi.org/10.1007/978-1-4419-9860-6_1.

Largitte, L., Pasquier, R., 2016. A review of the kinetics adsorption models and their application to the adsorption of lead by an activated carbon. Chem. Eng. Res. Des. 109, 495–504. https://doi.org/10.1016/j.cherd.2016.02.006.

Lim, S.-F., Lee, A.Y.W., 2015. Kinetic study on removal of heavy metal ions from aqueous solution by using soil. Environ. Sci. Pollut. Res. 22 (13), 10144–10158. https://doi.org/10.1007/s11356-015-4203-6.

Lu, W., et al., 2021. Adsorption and desorption characteristics of cadmium on different contaminated paddy soil types: kinetics, isotherms, and the effects of soil properties. Sustainability 13. https://doi.org/10.3390/su13137052.

Manzoor, M.A., et al., 2023. Environmental sustainable: biogenic copper oxide nanoparticles as nano-pesticides for investigating bioactivities against phytopathogens. Environ. Res. 231, 115941. https://doi.org/10.1016/j.envres.2023.115941.

Neira-Albornoz, A., et al., 2024. Understanding requirements, limitations and applicability of QSAR and PTF models for predicting sorption of pollutants on soils: a systematic review. Front. Environ. Sci. 12. https://doi.org/10.3389/fenvs.2024.1379283.

Neira-Albornoz, A., Fuentes, E., Cáceres-Jensen, L., 2022. Connecting the evidence about organic pollutant sorption on soils with environmental regulation and decision-making: a scoping review. Chemosphere 308, 136164. https://doi.org/10.1016/j.chemosphere.2022.136164.

Nkedi-Kizza, P., et al., 2006. Sorption kinetics and equilibria of organic pesticides in carbonatic soils from south florida. J. Environ. Qual. 35 (1), 268–276. https://doi.org/10.2134/jeq2005.0140.

OECD, 2000. Test no. 106: Adsorption-desorption using a batch equilibrium method. OECD Guidelines for the Testing of Chemicals, Section 1. OECD Publishing, Paris. https://doi.org/10.1787/9789264069602-en.

Qi, Z., Zhang, L., Chen, W., 2014. Transport of graphene oxide nanoparticles in saturated sandy soil. Environmental Science Processes Impacts 16 (10), 2268–2277. https://doi.org/10.1039/C4EM00063C.

Quesada-Peñate, I., et al., 2009. Comparative adsorption of levodopa from aqueous solution on different activated carbons. Chem. Eng. J. 152 (1), 183–188. https://doi.org/10.1016/j.cej.2009.04.039.

Rahman, M.S., et al., 2019. Arsenic(V) sorption kinetics in long-term arsenic pesticide contaminated soils. Appl. Geochem. 111, 104444. https://doi.org/10.1016/j.apgeochem.2019.104444.

Revellame, E.D., et al., 2020. Adsorption kinetic modeling using pseudo-first order and pseudo-second order rate laws: a review. Clean. Eng. Technol. 1, 100032. https://doi.org/10.1016/j.clet.2020.100032.

Rudzinski, W., Plazinski, W., 2007. Theoretical description of the kinetics of solute adsorption at heterogeneous solid/solution interfaces: on the possibility of distinguishing between the diffusional and the surface reaction kinetics models. Appl. Surf. Sci. 253 (13), 5827–5840. https://doi.org/10.1016/j.apsusc.2006.12.038.

Sadzawka, A., *Métodos de análisis de suelos*. Serie La Platina No. 16. 1991, Santiago, Chile: INIA.

Sadzawka, M.A.R., Aomine, S., 1977. Adsorption of silica in river waters by soils in central Chile. Soil Sci. Plant Nutr. 23 (3), 297–309. https://doi.org/10.1080/00380768.1977.10433049.

Salvestrini, S., et al., 2014. Modelling the biphasic sorption of simazine, imidacloprid, and boscalid in water/soil systems. J. Environ. Sci. Health Part B 49 (8), 578–590. https://doi.org/10.1080/03601234.2014.911575.

Sekine, R., et al., 2017. Aging of dissolved copper and copper-based nanoparticles in five different soils: Short-term kinetics vs. Long-term fate. J. Environ. Qual. 46 (6), 1198–1205. https://doi.org/10.2134/jeq2016.12.0485.

Sharma, N., Chaudhary, A., 2025. Assessing the role of soil amendments on the sorption-desorption behavior of glufosinate-ammonium herbicide in soils: kinetic, isothermal and thermodynamic investigations. Soil Sediment Contam. Int. J. 1–22. https://doi.org/10.1080/15320383.2025.2450397.

Tegenaw, A., et al., 2019. Characterization of colloid-size copper-based pesticide and its potential ecological implications. Environ. Pollut. 253, 278–287. https://doi.org/10.1016/j.envpol.2019.07.036.

Tomasgaard, L., J. Ringseth, and A. Bergkvist, *Granulated cuprous oxide for antifouling coatings*, in *U.S.P. Office, Editor*. 2004: United States.

Tran, H.N., et al., 2017. Mistakes and inconsistencies regarding adsorption of contaminants from aqueous solutions: a critical review. Water Res. 120, 88–116. https://doi.org/10.1016/j.watres.2017.04.014.

Vareda, J.P., 2023. On validity, physical meaning, mechanism insights and regression of adsorption kinetic models. J. Mol. Liq. 376, 121416. https://doi.org/10.1016/j.molliq.2023.121416.

Weber, Walter, J., Morris, J.C., 1963. Kinetics of adsorption on carbon from solution. J. Sanit. Eng. Div. 89 (2), 31–59. https://doi.org/10.1061/JSEDAI.0000430.

Wu, F.-C., Tseng, R.-L., Juang, R.-S., 2009a. Characteristics of elovich equation used for the analysis of adsorption kinetics in dye-chitosan systems. Chem. Eng. J. 150 (2), 366–373. https://doi.org/10.1016/j.cej.2009.01.014.

Wu, F.-C., Tseng, R.-L., Juang, R.-S., 2009b. Initial behavior of intraparticle diffusion model used in the description of adsorption kinetics. Chem. Eng. J. 153 (1), 1–8. https://doi.org/10.1016/j.cej.2009.04.042.

Zeldowitsch, J., 1934. Über den mechanismus der katalytischen oxydation von CO an MnO2. Acta Physicochim. URSS 1, 364–449.

Zhu, Q., Moggridge, G.D., D'Agostino, C., 2016. Adsorption of pyridine from aqueous solutions by polymeric adsorbents MN 200 and MN 500. Part 2: kinetics and diffusion analysis. Chem. Eng. J. 306, 1223–1233. https://doi.org/10.1016/j.cej.2016.07.087.